3D FLUORESCENT SPOTS DETECTION IN LINE-SCANNING CONFOCAL MICROSCOPY

E. Dusch[1,2], *N. Vincent*[1]

[1] SIP-CRIP5
Université René Descartes Paris 5
45, rue des Saints Pères, 75006 Paris, France

A. Genovesio[2]

[2] Image Mining Group
Institut Pasteur Korea
KIST, Seongbuk-gu, 136-791, Seoul, Korea

ABSTRACT

This paper describes a method to detect fluorescent PSF-like spots in 3d line-scanning confocal microscopy. We suppose that fluorescent spots are small enough to be characterized by the Point Spread function (PSF) of the microscope. To localize spots, we use a derivative expression of the image previously convolved by a Gaussian approximating the PSF. The algorithm validation is made on 3D synthetic images with fluorescent background structures and on a 3D fluorescent biological image.

Index Terms— Biomedical microscopy, 3D Point-Spread-Function, Line-Scanning Confocal Microscopy, Image object detection, Hessian operator.

1. INTRODUCTION

3D localization of biological particles is a major task for biologists to better understand intra-cellular processes. In a colocalization context, the idea is to locate spots relatively to the nucleus or to the cell in order to determine, for example, if a cell is infected [1]. Confocal microscopy enables to acquire, in two or more channels, 3d volumes of spots and cells tagged with different fluorescent dyes. Thanks to recent advances in microscopy systems, line-scanning confocal microscopy allows to record 3d volume faster and thus reduce undesirable phenomena like photobleaching or spots movement during the acquisition. Nonetheless an undesirable effect remains: highly fluorescent background structure can appear on the spot channel. Due to the diffusion of spot fluorescence within the cell and fluorescent dyes overlapping, it affects the detection process.

A classic method to detect spots is to associate them to local intensity maxima. Despite an adequate filtering to overcome the noise sensitivity [2], this approach is not well adapted to biological images with fluorescent background structures. A multiscale approach [3], based on an undecimated wavelet transformation of the image, allows to separate background structures from high frequency objects (noise and spots). Nevertheless, setting an automatic threshold of wavelet coefficient to discriminate between noise and spot remains an issue.

Differential approaches, commonly used for blob/spot detection, are derived from the Hessian operator of the image previously filtered by a Gaussian kernel. Operator response is strongly linked to the correlation between the Gaussian standard deviation and the expected spot size. Usually, a scale-space approach [4] is used in order to automatically catch spots of different and unknown size.

In our microscopy context, fluorescent particles are very small (0.05/0.2 μm) and can be considered as point sources. If we assume the microscope as being a shift invariant linear system, spots can be characterized by the impulse response of the microscope, the so-called Point Spread Function (PSF). With a Gaussian approximation of the PSF to determine the spot size, Thomann et Al. [5] used the Gaussian curvature to detect few fluorescent spots in widefield microscopy. Due to the special optic of line-scanning confocal microscopes (characterized by a line illumination in the object space and a slit-shaped line detector) [6], the line-scanning PSF differs from the widefield PSF. Based on the work of [5], we propose a score, adapted to the asymmetric shape of the line-scanning PSF, allowing to discriminate PSF-like spots from fluorescent background and noise.

The remainder of the paper is organized as follows. In section 2, a Gaussian approximation of a fluorescent line-scanning confocal microscope PSF is described. Our detection algorithm is detailed in section 3. Experimental results on synthetic and biological images are presented in section 4.

2. GAUSSIAN APPROXIMATION OF LINE-SCANNING PSF

In this section, we present a fluorescent line scanning confocal microscope PSF and its Gaussian approximation.

2.1. Line-scanning PSF model

Since the exact PSF is rarely known, many researchers have focused on modeling the PSF based on diffraction theory and knowledge of the optical microscope components (cf [7] and references within). A simplified scheme of fluorescent line-scanning microscope has been presented in [6]. In our model,

we consider, parallely to the x-axis, a line illumination generated on the sample plane by the objective lens and a line-shape detector (slit). Based on the Debye scalar theory, the 3D fluorescent line-scanning PSF can be written [8]:

$$h(x,y,z) = \left| \int_{-\alpha}^{\alpha} k_{ex} (\cos\theta)^{3/2} \exp\left(-ik_{ex} y \sin\theta - ik_{ex} z \cos\theta\right) d\theta \right|^2 \int_{-s}^{s} \left| \int_{0}^{\alpha} k_{em} \sqrt{\cos\theta} \sin\theta \exp(-ik_{em} z \cos\theta) J_0\left(k_{em} \sin\theta \sqrt{x^2 + (y-y_s)^2}\right) d\theta \right|^2 dy_s, \quad (1)$$

where $J_0(\mathbf{x})$ is the Bessel function of zero order. α is the maximal convergence semi-angle of the objective and is given by the objective numerical aperture NA$= n \sin\alpha$, with n the refractive index of the medium in which the objective is working. $k_{ex} = n\frac{2\pi}{\lambda_{ex}}$ and $k_{em} = n\frac{2\pi}{\lambda_{em}}$ are the excitation and fluorescence wavenumbers with the wavelengths λ_{ex} and $\lambda_{/em}$. s represents the half slit width in Airy unit (1AU$= \frac{1.22*\lambda}{\text{NA}}$M, where M is the objective magnification coefficient).

Under the assumption $\sin\theta \approx \theta$ and replacing θ by αt, it can be shown that Eq.(1) tends asymptotically to the paraxial model (NA inferior to 0.7) given in [6].

Figure 1 shows logarithm plots of the 3D PSF defined in Eq.1, where we choose s=0.25 AU, $\lambda_{ex} = 0.488\ \mu m$, $\lambda_{em} = 0.505\ \mu m$, n$= 1.51$ and NA$= 1.4$. The PSF along the line (x-axis) is equivalent to the widefield microscope PSF, while along the slit (y-axis) it is similar to a point-scanning confocal microscope PSF with typical pinhole sizes.

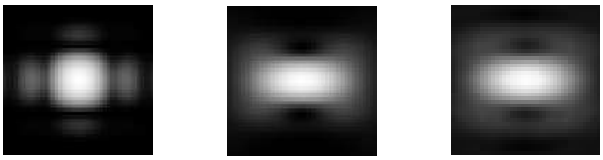

(a) xy-view (b) zx-view (c) zy-view

Fig. 1. Logarithmic plot of xy, zx, and zy views of the fluorescent line-scanning confocal PSF.

2.2. Gaussian approximation

Using non linear fitting, Thomann *et. al* [5] showed that the 3D fluorescent widefield PSF is well approximated by a Gaussian function. Zhang *et. al* [9] extended the work of Thomann to 3D fluorescent point-scanning confocal microscopes using Taylor series.

To approximate the line-scanning PSF defined previously, we use the following Gaussian function:

$$g_{\sigma_x,\sigma_y,\sigma_z}(x,y,z) = \exp\left(-\frac{x^2}{2\sigma_x^2} - \frac{y^2}{2\sigma_y^2} - \frac{z^2}{2\sigma_z^2}\right).$$

In this estimation problem, we want to find the Gaussian standard deviation that approximates best the PSF size. We minimize the usual least squares criterion to obtain an estimation of the set of Gaussian parameter $\sigma^* = \left\{\sigma_x^*, \sigma_y^*, \sigma_z^*\right\}$, i.e.:

$$\sigma^* = \underset{\sigma>0}{\operatorname{argmin}} \|\text{PSF} - g_\sigma\|_2^2 .$$

We use a non-linear least squares fitting algorithm [10] to obtain the parameters.

Using $\lambda_{ex} = 0.488\ \mu m$ and $\lambda_{em} = 0.505\ \mu m$, table 2.2 gives for typical slit sizes the standard deviation estimators in the object space (μm). Figure 2 shows the line-scanning PSF in x,y and z direction and its Gaussian approximation. Final standard deviations, used in the detection algorithm, are obtained by dividing these values by the sampling sizes.

We quantify the approximation error by measuring a relative squared error :

$$RSE = \frac{\|PSF - g_{\hat{\sigma}}\|^2}{\|g_{\hat{\sigma}}\|^2}.$$

Despite a high RSE for large slit sizes, figure 2 shows that the Gaussian approximation catches well the main lobe of the PSF in each direction. This standard deviation estimation is thus well adapted to a detection task.

	$NA = 1.4$			
	$\hat{\sigma}_x$	$\hat{\sigma}_y$	$\hat{\sigma}_z$	RSE
$s = 1$	0.071	0.076	0.177	0.14
$s = 0.5$	0.071	0.076	0.174	0.11
$s = 0.25$	0.070	0.073	0.164	0.06

Table 1. $\hat{\sigma}$ for NA$= 1.4$ and s$= 0.25, 0.5, 1$.

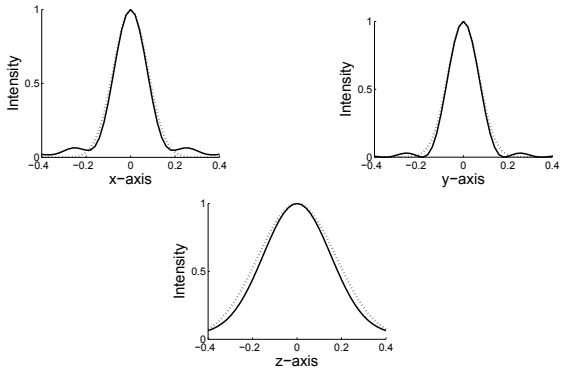

Fig. 2. x,y and z views of fluorescent line-scanning confocal PSF (solid line) and its Gaussian approximation (point line).

3. DETECTION PROCESS

This section describes a framework for extracting PSF-like fluorescent spots. Derived from the Hessian operator, the mean and Gaussian curvatures can be used to discriminate ridge and dome surfaces respectively[11]. Due to the asymmetry of the PSF (see figure 1), spots can not be considered as isotropic intensity surfaces. Hence, the mean curvature K should be well adapted.

To match the size of expected spots, we first perform a convolution of the image I with a Gaussian kernel g of standard deviation σ_g that approximates the line-scanning PSF. Then, we compute an operator response for each local maximum on the convolved image based on the mean curvature (trace of the Hessian, i.e the Laplacian of the Gaussian (LOG) of I):

$$K(I) = \Delta * (g * I) \tag{2}$$

where $*$ denotes convolution and Δ the Laplacian operator. Bright spots are characterized by a high negative response while noise and fluorescent background diffusion are represented by a near-zero response. We then use an otsu-type thresholding [12] approach based on the minimization of the within-class variance of the mean curvature distribution to classify spots.

4. EXPERIMENTAL RESULTS

In this section, we assess the performance of our approach on synthetic images and biological data.

4.1. Results on simulated images

In our simulations, we assume that fluorescent images are affected by two independent noises: shot noise and dark noise. Shot noise, arising from the statistical nature of photon production, leads to a Poisson noise with a variance equal to the number of detected photons. Dark noise, caused by the detector, can be modeled by a Gaussian distribution. In addition, we suppose that images have some fluorescent background structures. This imaging process can be expressed as :

$$I = P((o + b) * h) + w,$$

where I denotes the intensity observed, b is the background fluorescence and h is the PSF kernel defined by Eq. 1. P is a Poisson process with rate $\tau = (o + b) * h$ and w is the Gaussian noise of variance σ_N^2 :

$$\sigma = \frac{\overline{P((o + b) * h)}}{SNR},$$

where $\overline{(.)}$ denotes the mean and SNR is the signal to noise ratio in decibels (*db*).

We validate our algorithm on 30 synthetic images. To produce the original images, i.e before the imaging process, we simulate some spheres with a low gray level, b, to represent the fluorescent background and position N spots inside them. Spots size is one pixel and spots gray level is equal to 255.

Table 2 gives the ratio of true and false positive over the number of spots N for different values of SNR and b. Our algorithm performs well on simulated images until $b = 130$ and SNR $= 7$ db. These values correspond to a high level of noise and fluorescent background on real biological images. Regarding these results, our algorithm is robust for typical fluorescent biological images.

SNR\b	60	80	130	175	200	220
15	0.98	0.97	0.77	0.36	0.32	0.13
10	0.98	0.97	0.74	0.34	0.32	0.13
7	0.98	0.95	0.72	0.33	0.26	0.11
3	0.97	0.95	0.61	0.31	0.22	0.08

(a) true positive ratio

SNR\b	60	80	130	175	200	220
15	0	0	0	0.03	0.10	0.21
10	0	0	0	0.03	0.08	0.20
7	0	0	0	0.10	0.2	3.3
3	0	0	0	4.48	5.53	6.64

(b) false positive ratio

Table 2. Ratio of true and false positive over the number of spot.

Figure 3 shows detection results on three slices of a simulated volume with 39 spots. The spheres gray level for this simulation is equal to 130 and the SNR is fixed to 3 db. The sampling is $0.1\ \mu m$ in each direction and we used NA$= 1.4$, s=1, n$= 1.51$, $\lambda_{ex} = 0.488\ \mu m$ and $\lambda_{em} = 0.505\ \mu m$ to compute the PSF kernel.

4.2. Results on real images

We use for this validation a 3D biological image of proteins with typical fluorescent background. This image was acquired with the Zeiss LSM 5 live and is courtesy of the Dynamic Imaging Platform (Institut Pasteur Korea). Figure 4 shows three slices of this image and the corresponding detection.

5. CONCLUSION

We have presented in this paper a method to detect PSF-like spots in fluorescent line-scanning confocal microscopy. It involves a derivation of the Hessian operator and an approximation of the PSF by a Gaussian. Results demonstrate that our algorithm is robust up to a high level of fluorescent background and a low SNR. Yet, the proposed approach is not sufficient to detect spots separated by a distance below the

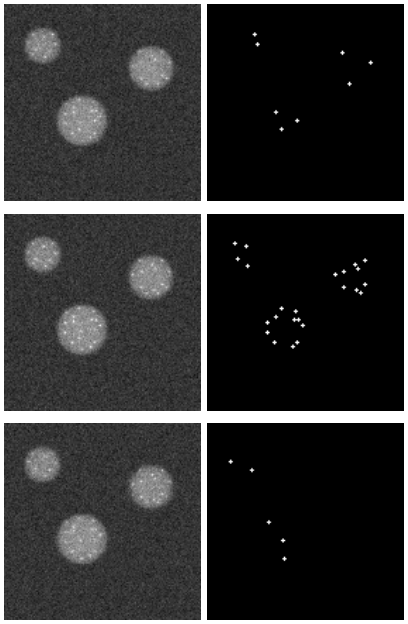

Fig. 3. Three slices of a simulated image (right) and the corresponding detection results (left)

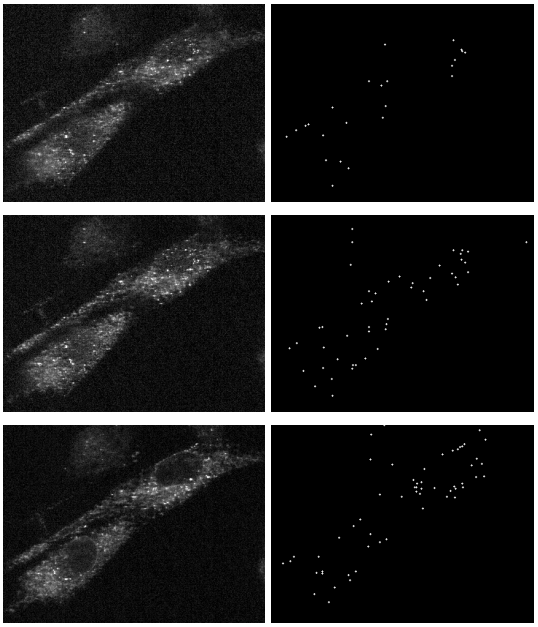

Fig. 4. Three slices of a protein image with typical fluorescent background (right) and the corresponding detection results (left).

microscope resolution limit (sub-resolution detection). This task will be the main consideration of our future works.

6. REFERENCES

[1] N. Arhel, A. Genovesio, K.A. Kim, S. Miko, E. Perret, J.-C. Olivo-Marin, S. Shorte, and P. Charneau, "Quantitative four-dimensional tracking of cytoplasmic and nuclear hiv-1 complexes.," *Nature Methods*, vol. 3, pp. 817–24, 2006.

[2] W. Tvarusko, M. Bentele, T. Misteli, R. Rudolf, C. Kaether, D.L. Spector, H.H. Gerdes, and R. Eils, "Time-resolved analysis and visualization of dynamic processes in living cells," *Cell Biology*, vol. 96, pp. 7950 – 7955, July 1999.

[3] J.-C. Olivo-Marin, "Extraction of spots in biological images using multiscale products," *Pattern Recognition*, vol. 35, no. 9, pp. 1989–1996, 2002.

[4] T. Lindeberg, "Feature detection with automatic scale selection," *International Journal of Computer Vision*, vol. 30, pp. 77–116, 1998.

[5] D. Thomann, D.R. Rines, P.K. Sorger, and G. Danuser, "Automatic fluorescent tag detection in 3D with super-resolution: application to the analysis of chromosome movement," *Journal of Microscopy*, vol. 208, no. 1, pp. 49–64, October 2002.

[6] R. Wolleschensky, B. Zimmermann, R. Ankerhold, and M. Kempe, "High-speed scanning confocal microscope for the life sciences," in *Confocal, Multiphoton, and Nonlinear Microscopic Imaging II. Proceedings of the SPIE*, T. Wilson, Ed., 2005, vol. 5860, pp. 87–94.

[7] M. Gu, *Advanced Optical Imaging Theory*, Springer-Verlag, Berlin, 2000.

[8] E. Dusch, T. Dorval, N. Vincent, and A. Genovesio, "3d point spread function model for line-scanning confocal microscope with high-aperture objective," Accepted in Journal of Microscopy.

[9] B. Zhang, J. Zerubia, and J.-C. Olivo-Marin, "A study of gaussian approximations of fluorescence microscopy psf models," in *Proceedings of SPIE*, 2006.

[10] W.H. Press, S.A. Teukolsky, W.T. Vetterling, and B.P. Flannery, *Numerical Recipies in C*, Cambridge University Press, 2nd edition, 1992, online book.

[11] R. C. Wilson and E.R. Hancock, "Consistent topographic surface labelling," *Pattern Recognition Letters*, vol. 32, pp. 1211–1223, 1999.

[12] N. Otsu, "A threshold selection method from gray-level histograms," *IEEE Transactions on Systems, Man and Cybernetics*, vol. 9, no. 1, pp. 62–66, 1979.